NUMERICAL MODELLING OF POROUS INJECTION IN A RADICAL FARMING SCRAMJET

Bianca R. Capra*, Russell R. Boyce*, Stefan Brieschenk*
***Centre for Hypersonics, The University of Queensland, Brisbane Australia**
b.capra@uq.edu.au; russell.boyce@uq.edu.au; s.brieschenk@uq.edu.au

Keywords: *Hypersonics, Scramjets, Radical Farming, Fuel Injection, Porous*

Abstract

A numerical investigation of the behaviour of fuel injection through a porous surface in an inlet-fuelled, radial-farming scramjet is presented. The performance of porous fuel injection is compared to discrete port hole injection at an equivalence ratio of $\phi \approx 0.4$ for both cases. The comparison is performed at a Mach 6.5 flow condition with a total specific enthalpy of 4.3 MJ/kg. The numerical results are compared to experiments performed in the T4 shock tunnel where available. The presented results demonstrate for the first time, that porous fuel injection has the potential to outperform port hole injectors in scramjet engines in terms of fuel-air mixing, ignition delays and achievable combustion efficiencies despite reduced fuel penetration heights.

1 Introduction

Demand for economical, safe and reliable access-to-space systems will continue to grow as the global economy becomes ever more reliant on space-based systems. A hybrid system, employing rocket and air-breathing technology, is the most likely candidate to meet this need. Such a system will require the scramjet engine component to operate in the Mach number range 8-12 at altitudes between 30-40km [18]. The key challenge in realising this system is to extend current scramjet technology so that appreciable sustained combustion and net thrust is achieved at these conditions. This paper presents results for one identified method of achieving this goal: improving the efficiency of the fuel injection process in an inlet-fuelled, radical-farming scramjet that has the potential to operate at Mach numbers >8.

Radical farming is a process that can augment combustion by generating combustion radicals such as OH, O and H in hot pockets of a supersonic combustor [9, 12]. Hot pockets within a supersonic stream form between the impingement points of reflected shock- and expansion waves at the combustor walls, as illustrated in Fig. 1. Scramjets designed to operate in radical-farming mode typically feature milder compression ratios, reduced combustor lengths and reduced overall skin friction drag while using fixed inlet/combustor geometries that allow operation in a wide range of Mach numbers.

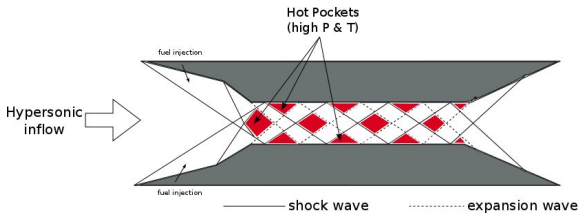

Fig. 1 : Schematic of radical farming process

The effectiveness of the radical farming process is strongly dependent on the fuel injection topology and resulting fuel-air mixing. Typically, fuel is injected via a series of discrete port holes located on the first or second intake ramp. Resulting interaction between the fuel jet and the hypersonic crossflow of this injection method causes

the formation of strong bow shocks [5, 21, 15, 20] which are accompanied by high total pressure losses. Other key drawbacks of port hole injection include flow separation both up- and downstream of the injector and limited fuel-air mixing [14].

These drawbacks can be overcome by employing porous media for fuel injection, rather than using discrete fuel injection ports. A recent preliminary study on the behaviour of porous fuel injection [16] in an inlet-fuelled, radical-farming scramjet, using the University of Queensland's T4 shock tunnel, has indicated significant increases in performance over discrete port hole injection. Figure 2(a) shows a schlieren visualisation of the intake flow of this experiment. It is clear from this result that the fuel / crossflow interaction causes a weak oblique shock at the point of injection rather than a strong bow shock. Figure 2(b) shows the combustor pressure traces for both, porous and port hole injection into Air and N_2. Both fuel injection methods resulted in combustion, as evidenced by the observed pressure rise for the fuel into Air shots compared with the equivalent fuel into N_2, and hence suppressed combustion shots. Porous injection, however, was found to produce a significantly higher combustion induced pressure rise within the combustor for the same fuelling levels, and thus resulted in an increase in performance.

The aim of this study is to gain more insight into the interaction physics between crossflow and porous fuel injection by numerical simulation using the Reynolds-Averaged Navier-Stokes (RANS) equations. The comparison between port hole and porous injection is made by conserving the global equivalence ratio as $\phi \approx 0.4$ for both cases.

2 Numerical modelling and computational model

The numerical simulations were performed using the CFD++ code from Metacomp Technologies [2]. Turbulence is modelled using the SST

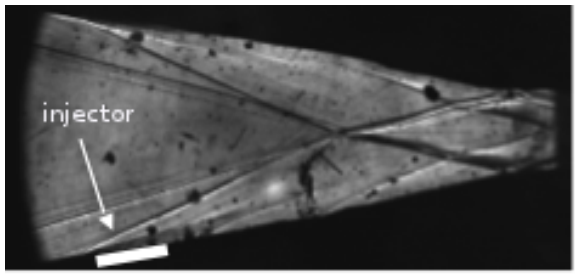

(a)

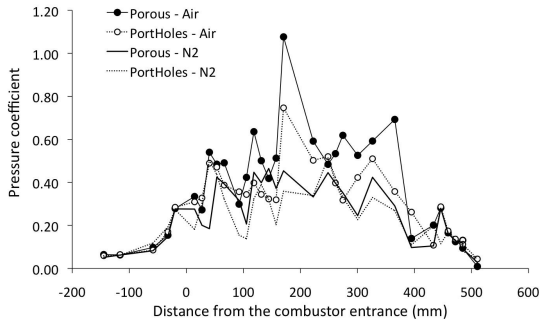

(b)

Fig. 2 : (a) Intake shock structure with porous injectors and (b) centre line pressure levels for porous and porthole injection (Schloegel [16])

k-ω turbulence model [10] with a 2% turbulence intensity and 1mm turbulent length scale. Computations were performed in double precision with second order accuracy. The Jachimowski-92 [6] finite-rate chemistry model was employed in these computations. This model considers 13 species and 33 reactions and is well suited to supersonic combustion studies [9, 1, 8].

The experimental model is inherently two-dimensional, however, the fuel injection topology requires simulation in 3D. A schematic of the 3D computational domain, including the applied boundary conditions, is given in Fig 3. The model measures 755.5 mm in length and consists of two inlet ramps with a combined horizontal length of 179.9 mm (139.9 mm first ramp, 45 mm second ramp) and total turning angle of 12° (9° and 3° respectively) and frontal capture area measuring 61.4 mm in height and 75 mm in width. The rectangular combustor measures 380.0 mm in length and 20.0 mm in height. The model has a thrust nozzle 195.6 mm in length with a diver-

gence of 9° [1]. Fuel injection was performed on the first intake ramp 95mm downstream of the leading edge using porous injectors. These injectors measured 44.4mm wide and 28mm long on the flow path side with a total thickness of 6mm and a 20° taper so that the plenum facing side was 10.1% larger in area than the flow path side. All porous injectors used in the experimental study were designed, manufactured and supplied by DLR Stuttgart and consisted of a Ceramic Matrix Composite (CMC) structure of carbon-carbon (C/C) with a porosity of approximately 16%.

The symmetrical nature of the engine has been exploited for this study such that only a quarter of the model was simulated with symmetry boundary conditions used were applicable. A fully structured mesh with ≈9x10^6 cells has been used in the computations. Cells were clustered towards the walls with an initial cell height of 1μm in order to capture the viscous sublayer without having to utilise wall functions. Clustering of the cells towards the flow entrance and exit of the porous injector was also necessary in order to correctly model the velocity profile of the flow through the injector. For the port hole fuel injection simulations, the porous injectors were replaced by four discrete 2-mm-diameter port holes resulting in an overall mesh of ≈1x10^7 cells.

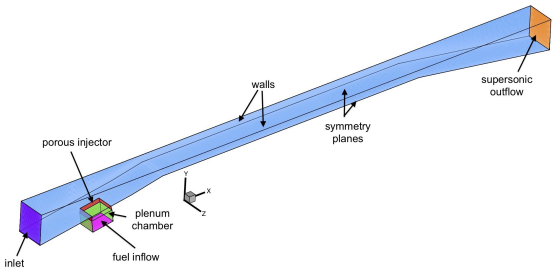

Fig. 3 : Numerical model for porous fuel injection studies.

The porous injector was computationally modelled as a discrete fluid block in which the porous source term given in Eq. 1 was applied to the momentum equations.

$$S_i = \left(\sum_{j=1}^{3} \mathbf{D}_{ij} \mu u_j + \sum_{j=1}^{3} \frac{1}{2} \mathbf{C}_{ij} \rho |u_j| u_j \right) \quad (1)$$

In this equation, the matrix coefficients $\mathbf{D_{ij}}$ and $\mathbf{C_{ij}}$ are user defined viscous and inertia terms used to characterise the porous structure. These are related to the Darcian - Forchheimer coefficients [3] of the examined porous sample by $\mathbf{D} = \frac{1}{K_D}$ and $\mathbf{C} = \frac{2}{K_F}$ respectively. The porous material used in the current study is anisotropic with coefficients reported to be: $K_{D_{xx}} = 1.079 \times 10^{-13} m^2$, $K_{D_{yy}} = K_{D_{zz}} = 7.584 \times 10^{-13} m^2$, and $K_{F_{xx}} = 8.065 \times 10^{-9} m^{-1}$, $K_{F_{yy}} = K_{F_{zz}} = 1.229 \times 10^{-7} m^{-1}$ [7]. All remaining coefficients were zero.

The computational domain includes the plenum chamber below the porous injector. This ensured the correct development of the flow profile prior to entering the porous injector and accounted for the development of boundary layers. Modelling of the plenum chamber was not performed for the porthole simulations where a sonic inflow condition was used instead.

3 Test Condition

Table 1 outlines the experimental test condition under which the scramjet was operated. The semi-empirical approach that is used to determine the total flow properties of the shock tunnel is discussed in detail elsewhere [1], but employs measured pressures and shock speeds in the facility shock tube to calculate the thermochemical equilibrium nozzle reservoir conditions.

The freestream properties given in Table 1 were determined using a 2D-axisymmetric RANS simulation assuming fully turbulent flow. Thermal equilibrium is assumed and the finite-rate chemistry is modelled using Park's [13] 5 species, 5 equation air-reaction scheme. Pressure, temperature and Mach number profiles at the exit of the contoured nozzle are shown in Figure 4. Core flow and capture area of the test engine have also

Table 1: Experimental freestream and stagnation conditions

property	value
p_s (MPa)	40.2
T_s (K)	3,378
h_0 (MJ/kg)	4.31
p_∞ (kPa)	8.99
T_∞ (T)	446
ρ_∞ (kg/m^3)	0.0699
u_∞ (m/s)	2,722
M_∞	6.44
ω_{O_2}	0.2050
ω_O	0. 0004
ω_{NO}	0.0500

been identified for reference. Results in this figure clearly show the non uniform flow structures present in the test gas, particularly towards the centre of the core flow corresponding to the volume ingested by the engine. It is important for the correct simulation of experimentally tested models that this non uniform freestream is included in engine analysis. The full profile of the non-uniform nozzle flow conditions has therefore been used in all subsequent analysis, however, freestream properties shown in Table 1 represent averages that were found over the intake capture area.

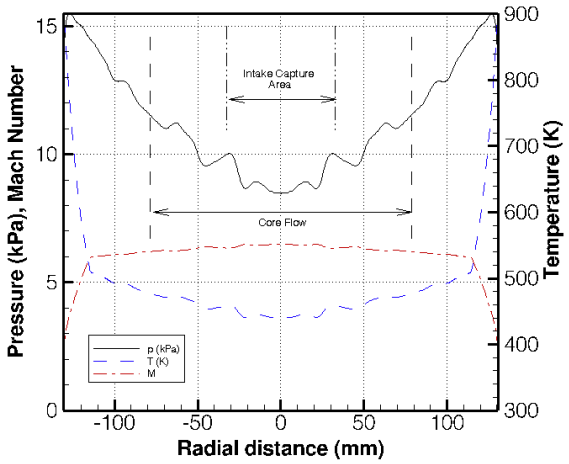

Fig. 4 : Nozzle exit profiles of flow properties.

4 Results

Although limited, comparison of the numerical results with the available test data, detailed in Section 4.1, indicates that the modelling, including the porous source term modelling, has adequately captured the key flow features observed experimentally. A level of confidence in the numerical model has therefore been demonstrated, allowing a more detailed assessment to be conducted on the numerical model that further probes the flow physics associated with porous fuel injection.

4.1 Comparison with Schlieren Visualisations

The numerical solution of the porous fuel injector has been compared to schlieren visualisations that were obtained during the experimental campaign. Fig 5 shows a composite image between the experimental schlieren image and the numerical simulation. The shock angles found from the schlieren visualisations match the shock angles found from the numerical simulations and indicate that the numerical implementation of the porous injection physics using Eq. 1 yields realistic results for the effect on the scramjet flow structure of the fuel exiting the porous wall.

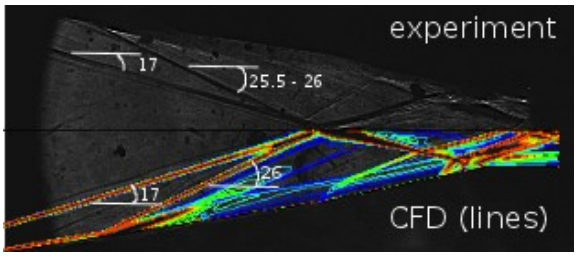

Fig. 5 : Experimental [16] and numerical schlieren for the porous fuel injector

4.2 Intake Shocks & Radical Farms

Shock wave structures obtained from the numerical simulations of equivalently fuelled porous

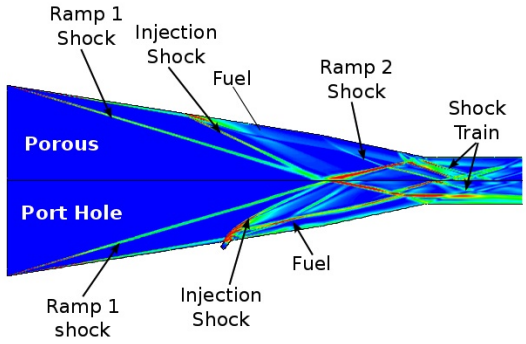

Fig. 6 : Numerical schlieren for porous and porthole injection

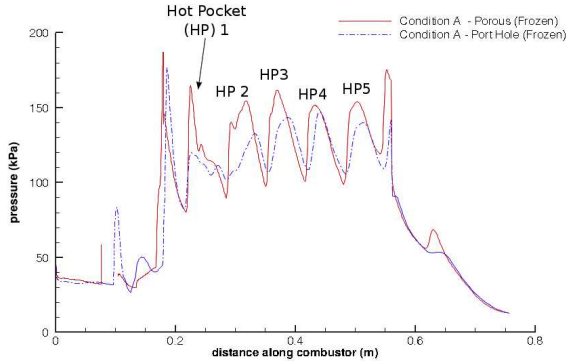

Fig. 7 : Frozen flow pressure distributions (centre line)

(top) and port hole (bottom) injectors are shown in Fig. 6. It is clearly evident from this figure that porous fuel injection alters both the intake and shock-expansion train structures characteristic of inlet fuelled port hole injection in radical farming engines.

The first, and most prominent, difference between the two simulations is the formation of an attached oblique shock wave at the point of injection with porous injection which replaces the detached bow shock associated with discrete port hole injection. This result confirms the injection shock characteristics first experimentally observed by Schloegel [16]. Formation of an oblique shock over a bow shock has many advantages for scramjets and supersonic combustion. First, being less severe, an oblique fuel injection shock is accompanied by lower total pressure losses as well as lower static pressure and temperature rises across the shock wave. Second, flow physics associated with the porous injector does not result in local flow separation, and the flowfield therefore does not show a reattachment shock. It is clear from this initial comparison, that porous fuel injection causes significantly lower flow disturbance and lower entropy losses.

Continuing the analysis of intake flow structures, the next key difference is in the location where the leading edge and injection shocks coalesce and interact with the flow from the second compression ramp. In the porous fuelled intake, these interactions are found to occur 3–4mm further upstream (Fig 6) resulting in a stronger shock-shock interaction propagating into the engine. The effect of this flow structure is an observed increase in pressure and temperature within the combustor hot pockets which are also shifted upstream as shown in Fig 7, where centreline wall pressure profiles for porous (solid red) and port hole (dashed blue) fuel injection are shown. Five distinct hot pockets (HP) can clearly been seen in this plot. The shift in peak pressure associated with porous injection, reflecting the shift of the radical farms due to the earlier shock-shock interaction, was found to range from 1mm for HP1 to 18 mm in HP3. Results from frozen simulations (suppressed combustion) are shown in this graph, therefore, all observed movement in the shock-expansion train is a result of the ingestion of the intake shocks and not associated with any heat release.

Peak temperature within the third near wall hot pocket for porous fuel injection is of the order 900K - 1,000K and is higher than the observed temperatures of the order of 800K for the port hole injection cases. This effect is due to the combination of the stronger shock-shock interaction and ‘warmer’ near wall conditions as a result of the improved mixing (to be discussed in Section 4.3). Pressure was also found to be higher in both the wall bounded and centreline hot pockets with porous injection, with the increase in pressure level seen to occur from the

first hot pocket. These flow features are a direct result of the oblique injection shock and stronger shock-shock interactions.

A higher and more uniform spanwise temperature and pressure distribution through the combustion chamber was also observed for the porous fuel injection case. Five distinct hot pockets form in the supersonic combustor, and it becomes clear from these results that the porous intake injection augments radical farming in the combustor through features such as the earlier formation of hot pockets that have both a higher temperature and pressure.

4.3 Fuel penetration, distribution & mixing

Fuel penetration and distribution within the engine from a point immediately aft of the injectors to the end of the combustion chamber for the two examined injection systems are shown in Fig 8. Finite-rate chemistry was deactivated in these simulations, thus the results presented highlight the mixing characteristics of the injection methods in the absence of combustion. Boundary layer edge location, defined as $U_e = 0.9U_\infty$, is also shown in this figure for a no fuelled (dashed black lines) and fuelled case (solid contours).

Porous fuel injection was found to result in more uniform fuel distribution, both in the spanwise (Fig 8(a)) and axial directions (Fig 8(b)). Fuel was also found to propagate further towards the side wall and into the corner regions, as early as 5mm downstream of the combustion chamber entrance, with porous injection. This is in contrast to the fuel distribution associated with port hole injection, which remains in discrete, fuel-rich tubes well into the combustion chamber that never spread into the side wall region. Two mechanisms cause the observed improved fuel distribution pattern. Firstly, porous injectors physically cover more surface area of the intake, thereby directly impacting the observed spread in fuel. Secondly, the injection interaction shock

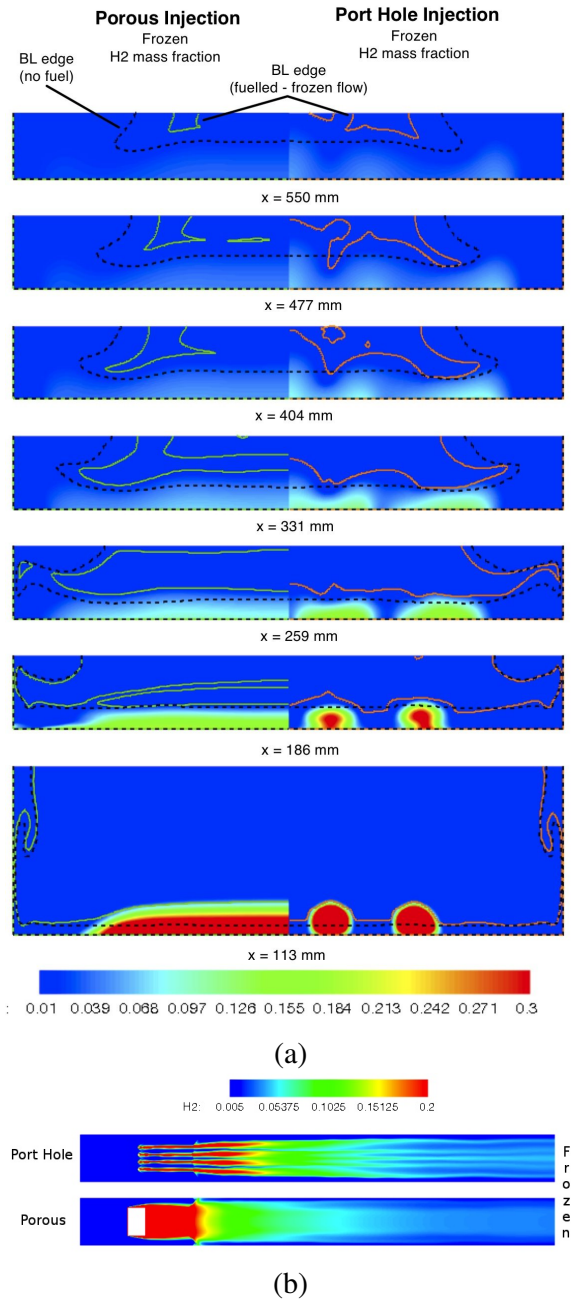

Fig. 8 : Fuel penetration for porous and port hole fuel injection (a) at axial locations within the engine and (b) along the wall

spans more uniformly across the intake.

Although fuel distribution, particularly in the wall region, was found to be improved compared with port hole injection, fuel penetration, based on classical definitions [17] was found to

be significantly reduced. Following the commonly employed criteria of fuel molar concentration of 99% [17] to define jet penetration resulted in negligible penetration height from the porous injector. Redefining the molar concentration limit to 90%, however, gives a penetration height of ≈2 mm at a distance of 113 mm from the leading edge, which is roughly 45% smaller as compared to port hole injection. Redefining the molar concentration limit to only 1% gives similar penetration heights for both, porous and port hole fuel injection (Fig 8).

Despite this perceived lack of fuel penetration, porous fuel injection was found to result in enhanced fuel/air mixing characterised by both a faster propagation and growth rate of the combustible mixture with porous fuel injection. This enhanced mixing subsequently reduced the fuel penetration height at the point of injection when based on techniques developed for port hole injection [17]. This is confirmed in Fig 9, which shows local equivalence ratio within the combustible range of $0.2 < \phi < 2$ [4] at consecutive axial locations. Both fuel injection methods result in significant fuel rich zones (red regions) immediately after the point of injection, with a thin layer of combustible mixture at the fuel/air interface. Further downstream of injection, however, porous injection results in a faster increase in the combustible region. This result is consistent with analytical predictions of mixing layer growth in a compressible turbulent shear/mixing layer given by Heiser and Pratt [4]. Following their method, mixing layer growth rates, $\frac{\delta_m}{x}$, for porous fuelled cases are approximately three orders of magnitudes higher as compared to port hole injection.

The enhanced spread and resultant mixing in the spanwise direction of the porous injection case is a result of the formation of a separated and recirculating flow region caused by the reflected shock interacting with the cool, thick, fuel jet just before the entrance of the combustion chamber. Mass transport via this separated recirculation region is a key mechanism to the overall ignition and ultimate combustion of fuel for the

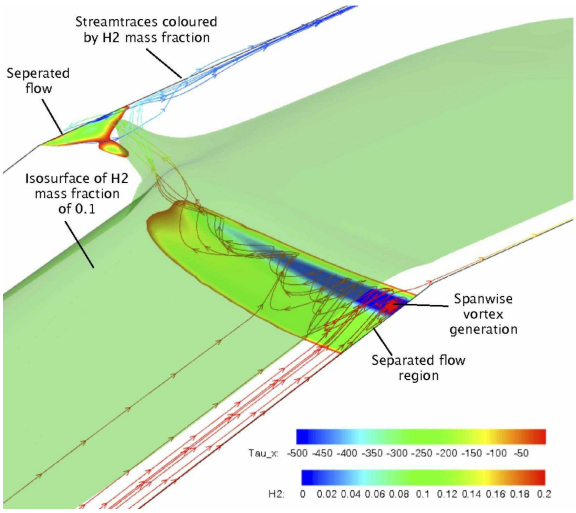

Fig. 10 : Separation region and spanwise vortex generation for porous injection that enables mass transport of fuel towards side walls

porous fuel injection case. The seperation creates a spanwise vortex that draws in fuel from the centre region and ejects it towards the side walls. The physically larger surface area associated with the porous injectors acts to increase the amount of fuel entrained within this vortex, compared with port hole injection which was found to exhibit a similar, but less pronounced, effect. Consequently, porous fuel injection was found to result in an increased level of fuel deposited towards the side walls. Furthermore, the fuel/air within this region was found to be better mixed with a greater volume of mixture in the combustable range.

4.4 Ignition & Combustion

For the observed enhanced mixing associated with porous injection to be effectively utilised in a radical farming scramjet, the local temperature and pressure within the mixing zone and hot pockets must be within suitable limits. Fig. 11 shows frozen contours of these variables for each injection method. Both fuel injection techniques are seen to result in an under-expanded and significantly cooled fuelled flow region which was found to equalise and reach a temperature approaching that for autoignition of H_2 - Air sys-

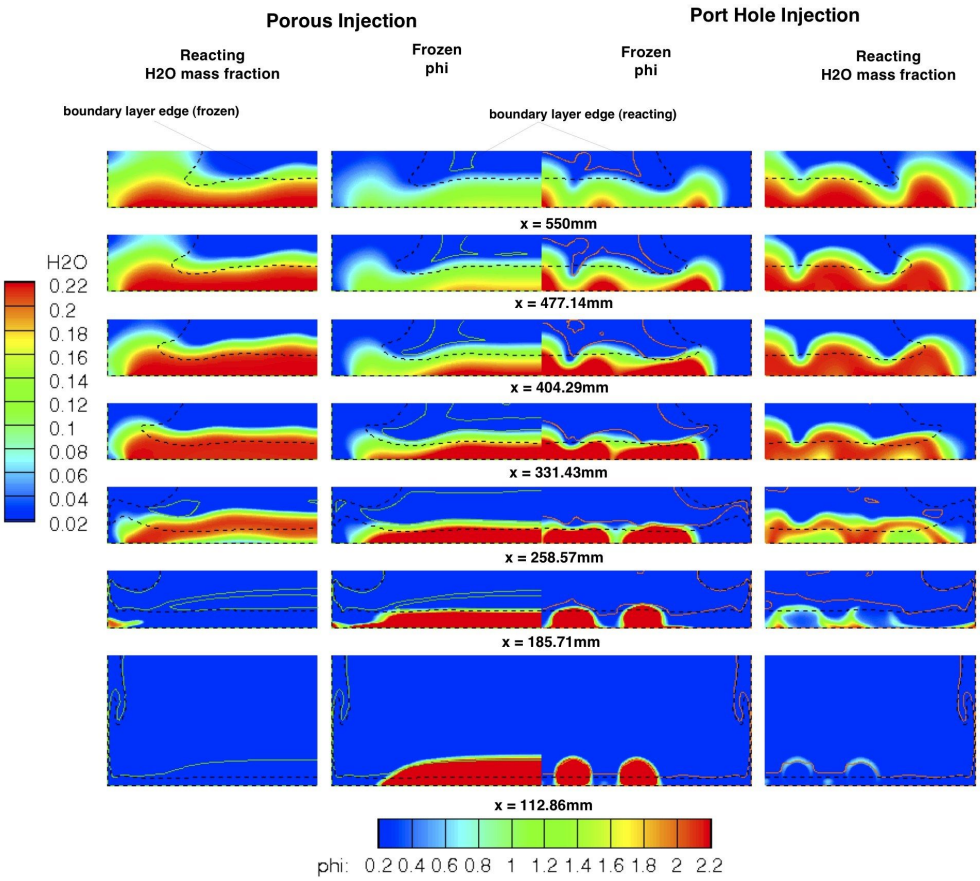

Fig. 9 : Local ϕ for chemically frozen flow with both porous and port hole fuel injection and resulting H_2O mass fraction for the chemically reactive simulation

tems [19] more rapidly with porous fuel injection. This is coupled with both the better mixing and more uniform higher pressures observed with porous injection. For the first two presented locations in the combustion chamber in Fig. 11 (x = 185.71mm and 258.57mm), the local side wall conditions are within the range 60–100 kPa and 1200 K for porous injection compared to 30–85 kPa and 1100 K for port hole injection.

Ignition behaviour, as indicated by the distribution of atomic hydrogen as well as combustion efficiencies, as indicated by the distribution of the H_2O molecule, are compared in Fig. 12. The strong interaction shock that is generated with port hole injection leads to small levels of radicals being produced on the intake, upstream of the combustor which are clearly identified in this

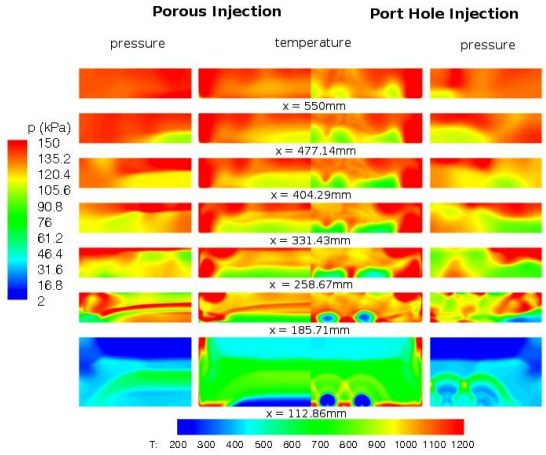

Fig. 11 : Frozen temperature and pressure contours at axial positions along the flow path for each injection method

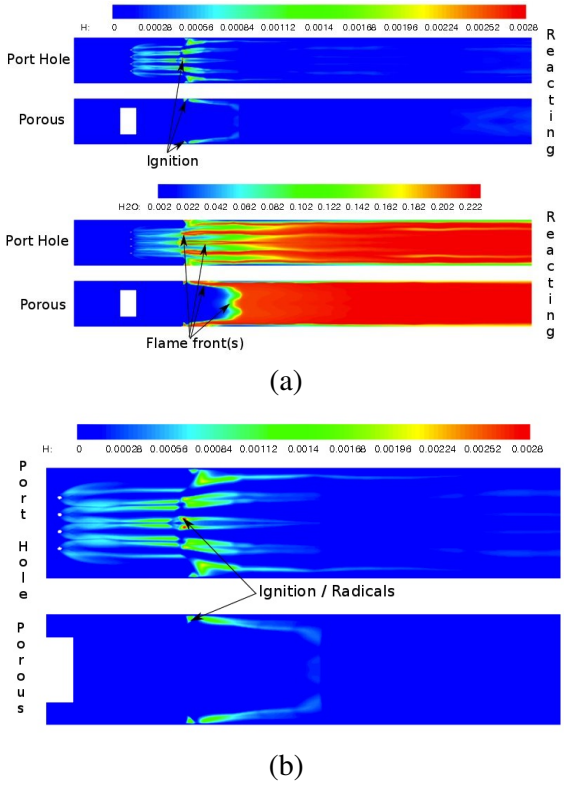

Fig. 12 : (a) H and H_2O for both injection methods and (b) close up of radical production at intake exit / combustor entry

figure. This is not the case, however, for porous injection where the interaction shock is weaker and thus insufficient to cause radical production on the intake.

The higher levels of fuel within the range $0.2 < \phi < 2.2$ existing in flow regions conducive to ignition leads to an observed reduction in ignition length for porous injection. Calculated using Nicholl's theory [11], ignition lengths at the symmetry plane, quarter model and 1.5mm from the side wall are given in Table 2. The ignition length for porous fuel injection is $\approx$ 20% lower as compared to port hole injection, except for the case of the quarter model location. Ignition length at the quarter model location, appears larger for porous injection. In this location, porous injection was found to have an ignition length of 83.7mm which was almost double that observed for port hole fuel delivery. A detailed analysis of the flow within this region

Table 2: Ignition length (mm)

Injection	Sym	$\frac{1}{4}$ Model	1.5mm from wall
Porous	78.6	83.7	8.76
Port Hole	91.1	41.4	11.42

for the two injection methods revels that this result is due to the way in which the air is entrained into the fuel jet in port hole injection. In this injection method, three distinct shear / mixing layers are developed between the injectors entraining fuel and air at combustible levels with small localised regions of high temperature and pressure caused by the bow shock generated upon fuel injection. Overall, however, the larger fuel spread and favourable mixing and ignitability conditions associated with porous fuel injection was observed to result in an overall decrease in ignition length.

Porous injection results in a flatter, thicker and more uniform combustion flame that is initiated in the separated region near the side wall before spreading uniformly towards the centre of the engine. This can be seen clearly by the formation of water in Fig. 12 and Fig. 9. Port hole injection, however, produces a series of discrete and streaked combustion flames, initiating within the shear layer between the fuel jets and at the side wall that then spread 'inwards' towards the fuel rich zone of the fuel jets. The effect of the observed changes in flame formation and propagation is a reduction in the length required to produce uniform H_2O production and therefore sustained combustion and heat release. For porous injection, uniform H_2O mass fraction along the combustion chamber wall was found to occur at x= 0.292mm which is 36% earlier than port hole injection. In addition, as shown in Fig 9, water production in the transverse direction is also more uniform and distributed for porous injection.

Porous fuel injection has a significant combustion augmentation effect on the scramjet geometry investigated in this work. This is more clearly shown in Fig. 13, where temperature and pressure distributions along streamlines 1 mm above

the start of the combustion chamber entry at the symmetry plane (a), quarter model location (b) and 1.5 mm from the side wall (c) have been plotted. Both fuel injection methods yield a high pressure rise and heat release within the second hot pocket, however, temperatures and pressures are higher for the porous injection cases.

5 Conclusions

This numerical investigation clearly shows that porous fuel injection can out perform the classical, discrete port hole injection. The numerical approach allowed the determination of the behaviour of porous injection on fuel-air mixing without the added complexity of combustion by probing the results from chemically frozen simulations. Computational results presented have shown that fuel injection through porous material enhances fuel-air mixing despite reduced fuel penetration heights.

This is due to both the larger surface area over which fuel is injected and the flow physics associated with porous injection. The presented computations have also shown that porous fuel injection yields weaker fuel jet / cross flow interaction shock structures and a stronger shock-/expansion-wave train travelling through the combustor. This has a positive effect on temperatures and pressures in the hot pockets and results in a higher combustor performance as measured by shorter ignition delays, increased heat release and a more uniformly propagating flame.

6 Acknowledgements

The authors would like to thank Mr Fabrice Schoegel for supplying experimental data used in this study, and Mr Markus Kuhn from DLR Stuttgart for information supplied about the physical properties of the porous injectors. This work was funded by the Australian Space Research Program (ASRP) as part of the SCRAMSPACE project and by computational resources provided

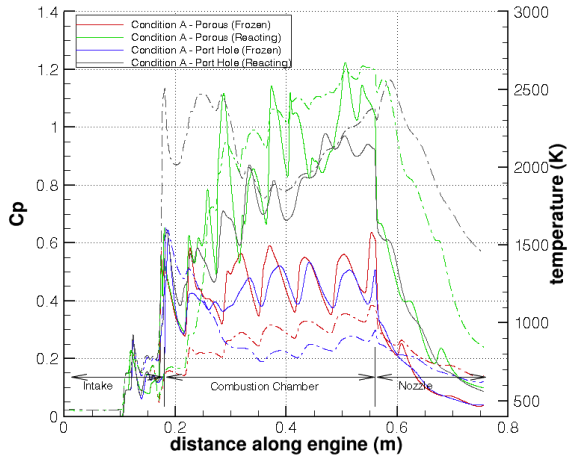

(a)

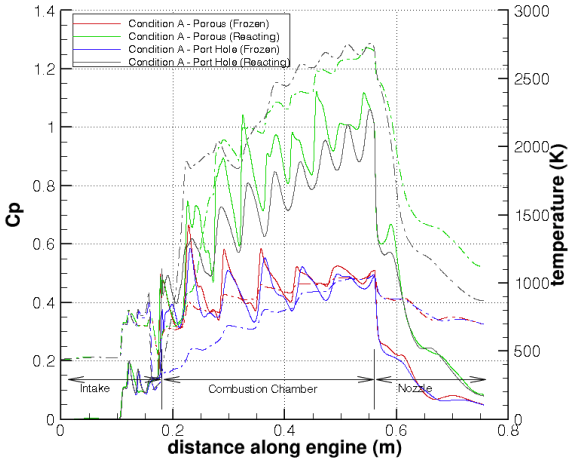

(b)

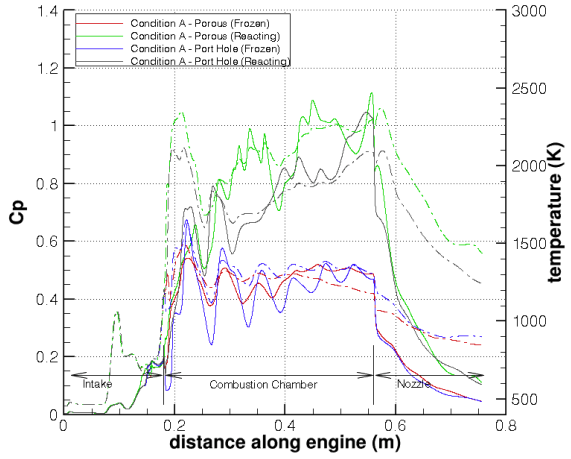

(c)

Fig. 13 : (a) symmetry, (b) quarter model and (c) 1.5mm from side wall

by Australia's National Computational Infrastructure (NCI) National Facility.

References

[1] R. R Boyce, F Schloegel, T. J McIntyre, and S. C Tirtey. Pressure-scaling of inlet-injection radical-farming scramjets. In *International Symposium on Airbreathing Engines*, Gothenburg, Sweden, September 2011.

[2] U Goldberg, O Peroomian, and Charkravarthy. Validation of cfd++ code capability for supersonic combustor flowfields. In *33rd AIAA/ASME/SAE/ASEE Joint Propulsion Conference and Exhibit*, Seattle, WA USA, 1997.

[3] H Hald, A Herbertz, M Kuhn, and M Ortelt. Technological aspects of transpiration cooled composite structures for thrust chamber applications. In *16th AIAA/DLR/DGLR International Space Planes and Hypersonic Systems and Technologies Conference*.

[4] William H. Heiser and David T. Pratt. *Hypersonic Airbreathing Propulsion*. AIAA Educational Series, 1994.

[5] S. D. Heister and A. R. Karagozian. Gaseous jet in supersonic crossflow. *AIAA Journal*, 28(5):819–827, 1990.

[6] C. J Jachimowski. An analysis of combustion studies in shock expansion tunnels and reflected shock tunnels. Nasa tp-3224, NASA, Langley, Research Center, July 1992.

[7] M Kuhn.

[8] P Lorrain, B.R Capra, and R.R Boyce. A detailed investigation of a nominally 2d radical farming scramjet combustion. In *abstract submitted to 18th International Space Planes and Hypersonic Systems and Technologies Conference*, 2012.

[9] J.R McGuire, R.R Boyce, and N.R Mudford. Radical-farming ignition processes in two-dimensional supersonic combustion. *Journal of Propulsion and Power*, 24(6):1248–1257, November/December 2008.

[10] F. R. Menter. *Zonal Two Equation k-w Turbulence Models For Aerodynamic Flows*. 24th AIAA Fluid Dynamics Conference, Orlando, USA, 1993.

[11] J. A Nicholls, T. C Adamson Jr, and R. B Morrison. Ignition time delay of hydrogen-oxygen-diluent mixtures at high temperaures. *AIAA Journal*, 1(10):2253–2257, October 1963.

[12] J. Odam and A. Paull. *Radical farming in scramjets*. in New Results in Numerical and Experimental Fluid Mechanics VI, Tropea, C., Jakirlic, S., Heinemann, H. J., Henke, R. and Hönlinger, H. (eds), Springer, Berlin, Germany, 2007.

[13] C Park. *Nonequilibrium Hypersonic Aerothermodynamics*. Wiley, New York, 1989.

[14] R. C. Rogers. *A study of the mixing of hydrogen injected normal to a supersonic airstream*. Technical note D-6669, NASA Langley Research Center, Hampton, USA, 1971.

[15] J.A Schetz and F.S Billig. Penetration of gaseous jets injected into a supersonic stream. *AIAA Journal of Spacecraft and Rockets*, 3(11):1658–1665, November 1966.

[16] F Schloegel. unpublished data, 2010.

[17] Corin Segal. *The Scramjet Engine, Processes and Characteristics*. Cambridge University Press, 2009.

[18] M. K. Smart. *Scramjets*. NATO-RTO-AVT, Rhode-Saint-Genèse, Belgium, 2008.

[19] C.J Sung, J.G Li, G Yu, and C.K Law. Chemical kinetics and self-ignition in a model supersonic hydrogen-air combustor. *AIAA Journal*, 37(2):208 – 214, February 1999.

[20] V Viti, R Neel, and J.A Schetz. Detailed flow physics of the supersonic jet interaction flow field. *Physics of Fluids*, 21(4), 2009.

[21] E.E Zukoski and F.W Spaid. Secondary injection of gases into supersonic flow. *AIAA Journal*, 2(10):1689–1696, October 1964.

6.1 Copyright Statement